# The effect of structural porosity on the ablation of sea ice ridges

Trisha L. Amundrud,[1,2] Humfrey Melling,[3] R. Grant Ingram,[1] and Susan E. Allen[1]

Received 21 January 2005; revised 20 July 2005; accepted 3 February 2006; published 1 June 2006.

[1] Observations reveal that the decrease in ice thickness through melting in summer is much more rapid for ridges than for surrounding level ice. A physical model that represents internal melting within ridge keels has been developed to explain this observed draft-dependent ablation for first-year pack ice in the Beaufort Sea. The porous structure of a ridge keel permits percolation of a substantial fraction of the oncoming oceanic flow, up to 20% for a feature with 30% porosity and 9-m draft. The percolating flow delivers oceanic heat to a large surface area deep within the keel and increases melt rates relative to surrounding level ice by a factor of 5 when seawater temperatures are 0.18 degrees above freezing. Melt rates are sensitive to the internal geometry of ridges through keel porosity and block dimensions, characteristics that vary widely between ridge features. However, the average rate of melting as a function of draft, calculated for a realistic population of keels with average cross-sectional shape and differing draft, has the same draft-dependence as the observations. This concurrence suggests that the process of internal melting may be dominant in the ablation of ridged ice. In addition, internal melting during the summer may well hasten structural consolidation of surviving ridge keels through freezing during the following winter. It appears that the evolution of the thickest ice within the Arctic ice pack is dependent on the small-scale structural characteristics of the ridged ice and its interaction with the upper layer of the ocean.

**Citation:** Amundrud, T. L., H. Melling, R. G. Ingram, and S. E. Allen (2006), The effect of structural porosity on the ablation of sea ice ridges, *J. Geophys. Res.*, *111*, C06004, doi:10.1029/2005JC002895.

## 1. Introduction

[2] The fate of global sea ice in the face of a generally warming climate is a current area of concern. However, realistic predictions of future ice cover require an understanding of the present pack ice; its extent, thickness, and variation on seasonal and longer timescales. Pack ice is a complex aggregate of level floes, ridges of recently fractured ice blocks, thermally weathered features, and ice-free leads. These elements respond differently to changes in ocean temperature, air temperature, snowfall, cloud cover, and ice circulation induced by changing climate. Of these four elements, sea-ice ridges can contain as much as 70% of the total pack-ice volume [*Melling and Riedel*, 1996]. Therefore to improve understanding of the fate and future extent of the global ice cover, there is a strong incentive to elucidate the physics both of the formation and the decay of ridged features. In recent work we have shown that certain geometrical properties of pack ice, namely the thickness and extent of level floes and the shape of ridges, are important factors in determining changes in the probability distribution of ice thickness during ridge building [*Amundrud et al.*, 2004]. In this paper we reach a similar conclusion in regard to the ablation of thick ridged ice: Geometrical details of ridge structure are important determinants of the ablation rate of ridged ice and the resulting change in the ice-thickness distribution during summer.

[3] Observations have consistently indicated that ridges in pack ice melt more rapidly and perhaps under a wider range of conditions than level floes. During a yearlong occupation of a floe drifting across the Beaufort Sea, repeated measurements of thickness at selected sites by *Rigby and Hanson* [1976] revealed enhanced ablation of ridged ice in comparison to level ice. *Wadhams* [1992], using data from submarine sonar, documented a progressive decrease in the occurrence of thick ice along a transect following the direction of ice drift from the North Pole to the East Greenland shelf. *Melling* [2002] revealed a similar thinning tendency in the pack ice along the path of drift through the Canadian Archipelago, by mapping data acquired by drilling over a 10-year period in the 1970s.

[4] Recent attempts to explain the enhanced melting have explored the interaction of the keel shape with the flow in the upper layer of the ocean. *Schramm et al.* [2000] used a numerical model to study the importance of two-dimensional heat conduction and the increased basal surface area of a triangular ridge section on the enhanced melt of ridged ice. However, these mechanisms were found to account for only a small fraction of observed melt. *Skyllingstad et al.* [2003] modelled the influence of ice keels on the hydraulics

[1]Department of Earth and Ocean Sciences, University of British Columbia, Vancouver, British Columbia, Canada.
[2]Now at Fisheries Research Services Marine Laboratory, Aberdeen, UK.
[3]Institute of Ocean Sciences, Department of Fisheries and Oceans, Sidney, British Columbia, Canada.


0148-0227/06/2005JC002895$09.00

and turbulence of under-ice flows. They found the disturbance of flow by ice topography was capable of significantly enhancing the flux of sensible heat to the ice in the vicinity of keels. In one simulation of flow beneath a keel of 10.8-m draft at the SHEBA (Surface Heat Budget of the Arctic Ocean, March 1998) site, the current at the keel crest was amplified five times relative to the undisturbed flow. For a freezing-temperature departure of 0.05°C and a relatively rapid 20-cm $s^{-1}$ flow, the heat flux was 120 W $m^{-2}$ on the upstream face of the keel and 40 W $m^{-2}$ on the downstream face. Although these are large values, their overall significance is difficult to assess from this study; only a few events were simulated, and the hydraulic interactions of flow with topography vary greatly with Froude number [*Pite et al.*, 1995]. It is also unclear whether this mechanism causes ablation that varies with draft in the manner observed.

[5] We present an argument that percolation of warm seawater into the porous structure of ridge keels can greatly enhance the ablation of these features relative to surrounding level floes. Young ridges are open structures of loosely stacked ice blocks within an envelope of irregular shape. The measured fractal dimension of this envelope is close to 2.5 [*Melling et al.*, 1993; *Melling and Riedel*, 1995; *Bowen and Topham*, 1996], indicating an extremely rough surface and a high surface area to volume ratio. This high fractal dimension is the surface manifestation of a porous internal structure; water-filled cavities in first-year ice ridges comprise 20–45% of the volume within the envelope [*Bowen and Topham*, 1996], with average porosities of 30% [*Timco and Burden*, 1997]. Fundamentally, the important effect of porosity in relation to ablation is the dramatic increase in the ice-surface area within the keel envelope. This increase in surface area amplifies the relatively small conductive heat transfer through a solid keel that was calculated by *Schramm et al.* [2000]. A secondary effect is the reduced volume of ice within the envelope of an unconsolidated keel; an average 30% less ice must be melted per unit reduction in draft than for a solid ice feature.

## 2. Ablation of Ridged Ice

### 2.1. Observations of Ice Evolution in the Beaufort Sea

[6] The draft of pack ice in the Beaufort Sea has been routinely measured by ice-profiling sonar (IPS: Institute of Ocean Sciences, Sidney, British Columbia) along with measurements of ice velocity from acoustic Doppler current profiler (ADCP: RD Instruments, San Diego, California) on subsea moorings since 1990 (Figure 1a). Statistical distributions of ice draft with a useful level of confidence can be calculated from observations of draft and ice movement accumulated over approximately 50 km of drift [*Melling and Riedel*, 1995]. Ice velocity measured at the mooring provides estimates of the relative motion of the ice pack above the mooring (Figure 1b). The displacement of pack ice (a Lagrangian quantity) has been approximated here by the integral of the ice velocity at the mooring (an Eulerian quantity). If the natural motion of the pack returned exactly the same area across the mooring at a later time, observations of the evolution of the ice draft distribution would be possible.

[7] In a more common ice-motion event, an area of pack ice is driven landward and then seaward, while moving in an along-shore direction. In general, the organization of a coastal ice field in bands that run parallel to the shore [*Melling*, 1998] allows an assumption of alongshore homogeneity in the statistical properties of the pack [*Amundrud et al.*, 2004]. With onshore and offshore motion (Figure 1b) superimposed on a general westward drift, the ice that moves back over the moorings was formed further to the east than the original, but nonetheless from the same band as that initially viewed. With this assumption the time-dependent evolution of a zone of pack ice can be estimated.

[8] There were four events during the warm season of 2000 when an ice zone was observed more than once by the sonar (Figure 1b). Observations of the thinning of level ice during these events reveal a consistent decrease in draft that supports the assumption of alongshore homogeneity in the first-year ice population of this region.

### 2.2. Evidence for Enhanced Melting

[9] During the summer, melt processes lead to a general decrease in the draft of pack ice. However, there may be temporary interruptions of this general trend caused by the creation of new ridges during summer storms. For this reason, an estimate of the ablation rate derived from successive measurements of the ice-draft distribution will be a lower bound to the actual value, since the impact of ridging in increasing the average draft has been neglected. *Amundrud et al.* [2004] have simulated the redistribution of pack-ice draft in response to measured strain under wintertime conditions. However, not enough is known about the reduction in the strength of sea ice in summer [*Johnston and Frederking*, 2001] to utilize this approach here. We therefore will use the lower bound to the ablation rate that is derived from measurements during events depicted in Figure 1b.

[10] The ablation rate of ridged ice can be calculated from sequential observations as the rate of change of draft at fixed percentiles of the cumulative distribution of draft. The cumulative distribution is defined for this purpose as the proportion of ice that has draft greater than or equal to the reference value, in contrast to the conventional definition, which integrates from the lower limit. We have referenced the observed ablation rate to the average of the initial and final draft values at the selected percentile.

[11] Ablation rates during the events identified in Figure 1b are plotted against draft in Figure 2. During all events there is general increase in melting rate with draft. The rate for the short-lived event C has been calculated by comparing data from events B/C combined and C/D combined in order to achieve better statistical confidence. During event D (July 2000) the observed thinning of level ice was approximately 2–3 cm $d^{-1}$, while the observed ablation of keels was as rapid as 15 cm $d^{-1}$.

[12] Uncertainty in the rate of ablation has been estimated using the limits of confidence for the empirical distribution of draft, following *Rothrock* [1986] and *Melling and Riedel* [1995]. Limits based on adding the uncertainties have been plotted on Figure 2. This error is a generous overestimate, as the error in the initial and final cumulative density profiles should be independent, and thus should scale in quadrature. Clearly, imprecision in the calculated rate of ablation does

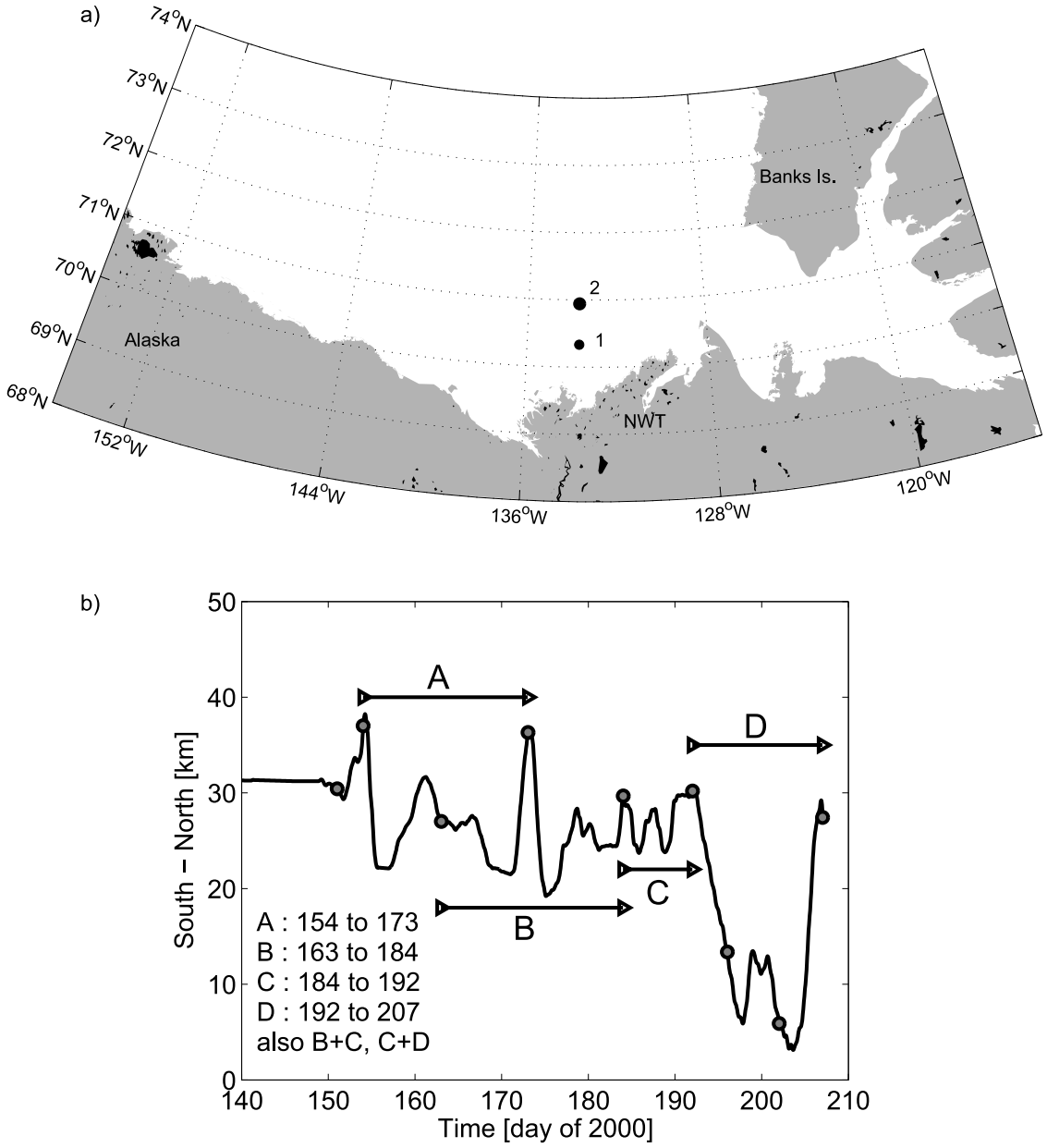


**Figure 1.** (a) Mooring sites in the Beaufort Sea (black shading indicates lakes). (b) North-South Eulerian displacement illustrating ice motion over mooring site 2 during the first half of 2000. Origin of vertical scale is arbitrary. Observed ice draft distributions are centered at points indicated by circles on the path. Ablation begins around day 150 and four ice motion events are identified where the ice moves in an onshore-offshore pattern (indicated as A, B, C, and D).

not change the conclusion that ridged ice thins much more rapidly than level ice.

### 2.3. Characteristics of the Upper Ocean Under Ice

[13] The basic physics of sea-ice ablation through oceanic influence is dependent upon the departure from freezing temperature in the upper ocean and on the relative motion of the under-ice boundary layer. Although we have no upper ocean data from the Beaufort Sea during the early summer of 2000, data from other years and locations can provide typical ranges of value for these parameters.

[14] An ADCP drifting with the pack over the Beaufort shelf (70.5°N, 132°W) during five days in April 1989 measured a relative current of 6.9 cm $s^{-1}$ at 10-m depth when the ice was drifting at about twice this speed (H. Melling, unpublished data, 1989). Other data from the SHEBA camp during the summer of 1998 (near 80°N, 165°W) indicate relative flows of 10 cm $s^{-1}$ at 4-m depth in June and 15 cm $s^{-1}$ at 2-m depth in July [*McPhee*, 2002]. Unfortunately, because the sensors used could not detect flow slower than 5 cm $s^{-1}$, these average values may be biased high. For this discussion, we have chosen a relative

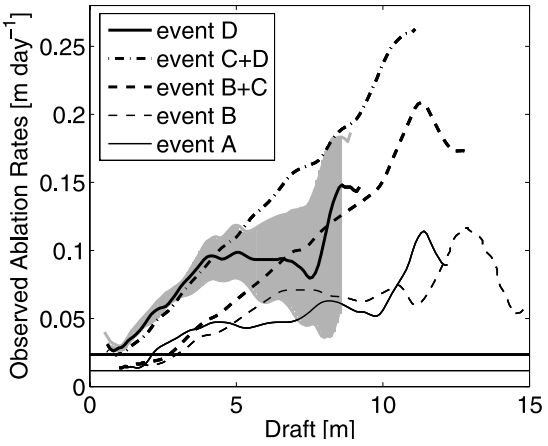


**Figure 2.** Observed ablation rate as a function of draft during the ice motion events in Figure 1b. Level ice melt rates for events A and D are indicated as the solid thin and thick horizontal lines, respectively. Observed error in melting rate for event D is indicated as the shaded region, which represents the maximum error using one standard deviation from the cumulative distribution. Both level ice melting rates and ridged ice ablation rates increase throughout the ablation season.

oceanic flow at 10 cm s$^{-1}$ aligned randomly relative to the keel axis. The average component of speed across a randomly orientated group of keels is 6.3 cm s$^{-1}$, the average of 10 cos θ over angle from 0 to a value near 90°. The relative flow will decrease from 10-m depth toward the ice, reflecting frictional effects and the nonslip boundary condition at the ice-ocean interface. However, for simplicity we assume that the current speed is a uniform 6.3 cm s$^{-1}$ over the depth range occupied by the keels (Table 1).

[15] Without any observations of ocean temperature at our mooring sites, a reasonable guess for the temperature of the upper layer of the ocean can be made by looking at other data sets. Profiles of temperature and salinity in the ocean were measured routinely at the SHEBA site (data source: http://sheba.apl.washington.edu/) through operation of a fully automated winch, CTD probe, and acquisition system. During much of the summer of 1998 the upper 15-m of the water column was uniform in temperature and salinity. The average freezing temperature departures within the oceanic boundary layer over ten-day intervals centered at days 155 to 205 were 0.07, 0.08, 0.11, 0.14, 0.18, and 0.26°C degrees, respectively. For our calculations, we have chosen a boundary-layer temperature 0.18°C above freezing, the average value for the period beginning on day 195 (12 July) in 1998 (Table 1). This represents a best-guess value and is used to demonstrate the potential for internal melt to contribute to the enhanced melt.

## 3. A Model of Thermal Ablation Within an Ice Keel

### 3.1. Percolating Flow Through a Ridge Keel

[16] The fractal envelope of ridged ice is the external manifestation of its internal porous structure. Flow through porous media is well studied in groundwater and engineering disciplines, and results can be adapted to ridged ice. We define the direction $\hat{x}$ to be across the ridge and permit the oceanic flow to approach from any direction in the horizontal plane. However, within the keel we consider only the component of the incident flow that moves on average in the $\hat{x}$ direction.

**Table 1.** Parameters and Constants Used in Internal Ice Ablation Model[a]

| Symbol | Parameter Name | Value | Reference |
|---|---|---|---|
| | | *Physical Parameters* | |
| $h$ | block thickness | 0.5 m | section 5.1 |
| | block width, block length | 2.33$h$, 1.26$h$ | *Sayed and Frederking* [1989] |
| $p$ | porosity | 0.3 | *Lapparanta et al.* [1995] |
| $U$ | ocean velocity, relative to ice | 0.1 m s$^{-1}$ | 1989 data[b] |
| $T_o$ | ocean temperature above freezing | 0.18°C | SHEBA data set[c] |
| $W$ | keel width | 6.8$H$ | section 5.1 |
| λ | keel shape | 0.50$H$ − 0.30 m | section 5.1 |
| | | *Empirical Parameters* | |
| λ, β | Forchheimer coefficients | 20, 0.11 | *van Gent* [1995] |
| $C_D$ | drag coefficient | 3.5 | *Pite et al.* [1995] |
| Nu | Nusselt number | 0.023 Re$^{0.8}$ Pr$^{1/3}$ | *Bird et al.* [1960] |
| Pr | Prandtl number | 13.6 | *Holland and Jenkins* [1999] |
| Re | Reynolds number | 4R$_H$u/$\nu$ | *Bird et al.* [1960] |
| | | *Physical Constants* | |
| $\nu$ | kinematic viscosity of seawater | 1.8 × 10$^{-6}$ m$^2$ s$^{-1}$ | |
| $c_P$ | heat capacity of seawater | 4218 J kg$^{-1}$ | |
| κ | thermal conductivity of seawater | 0.56 J m$^{-1}$ | |
| $L_i$ | latent heat of fusion for ice | 334,000 J kg$^{-1}$ | |
| ρ, ρ$_i$ | densities of seawater and ice | 1024 kg m$^{-3}$; 920 kg m$^{-3}$ | |

[a]Physical parameters refer to the chosen values for keel geometry and ocean characteristics and represent reasonable values.
[b]Unpublished observations of H. Melling, 1989.
[c]SHEBA data available from http://sheba.apl.washington.edu/. Empirical parameters are chosen to best represent the ice keel system on the basis of observations. Physical constants are given for reference.

[17] Darcy's Law is often used to describe the speed of flow through a fluid-filled porous medium and is valid when the Reynolds number, Re, is less than 1, which holds true for most groundwater systems. However, flow at a speed of 0.5–2.5 cm $s^{-1}$ through an ice keel with pores of 1- to 20-cm scale (values estimated later in this paper) has a Reynolds number in the 25–3000 range, beyond that appropriate to Darcy's Law. An extension to Darcy's Law for slightly turbulent flows, the Forchheimer equation, includes an inertial component [*Burcharth and Andersen*, 1995] and relates the discharge flow to the hydraulic gradient $I_H$. The latter is proportional to the pressure gradient through the medium in the direction $\hat{x}$ [*Batchelor*, 1967, p. 224]:

$$-\frac{1}{\rho\, g}\frac{\partial P}{\partial x} = I_H \tag{1}$$

Here $P$ is pressure, $\rho$ is the density of seawater, and $g$ is the gravitational acceleration.

[18] The Forchheimer equation is derived from the Navier-Stokes equation for one-dimensional, steady, nonrotational flow [*Burcharth and Andersen*, 1995]. From the Navier-Stokes equation [*Gill*, 1982] written in terms of the hydraulic gradient (1), neglecting time-dependent terms, we obtain

$$-\frac{1}{\rho\, g}\frac{\partial P}{\partial x} = -\frac{\nu}{g}\frac{\partial^2 u}{\partial x^2} + \frac{u}{g}\cdot\frac{\partial u}{\partial x} \tag{2}$$

[19] On the right hand side the first term represents viscous effects where $\nu$ is the kinematic viscosity of seawater ($1.8 \times 10^{-6}$ $m^2$ $s^{-1}$), and the second term represents inertia. Following *Burcharth and Andersen* [1995], we obtain the Forchheimer equation by defining characteristic length and velocity scales for the flow through the pores. The characteristic pore length is the hydraulic radius, $R_H$, defined as the ratio of the volume of pores to their surface area. The derivation of *Burcharth and Andersen* [1995] assumes that the medium is composed of spherical granules. Our ridge is built from rectangular ice blocks of thickness $h$ and ratios of length and width to thickness equal to $b_1$ and $b_2$. For rectangular granules $R_H$ can be written as [*Amundrud*, 2004]:

$$R_H = \left(\frac{p}{1-p}\right)\frac{b_1 b_2 h}{2(b_1 b_2 + b_1 + b_2)} = \frac{ph}{(1-p)\gamma} \tag{3}$$

[20] The factor $\gamma$ is a geometrical factor related to the shape of the blocks forming the keel. *Sayed and Frederking* [1989] measured the length and width ratios to thickness of ice blocks in the sails of land-fast ice ridges. For their average values of 2.33 and 1.26, $\gamma$ is 4.45. The factor $p/(1-p)$ is the ratio of the fluid to solid volumes within the keel where $p$ is the porosity.

[21] In this analysis, the porosity, $p$, of the lower portion of the keel is assumed to be 0.3 and uniform [*Lepparanta et al.*, 1995]. With this porosity, the hydraulic radius is $R_H$ = 0.096 h. If the keel was built 10-cm thick ice, the hydraulic radius is 0.96 cm; for 1-m thick blocks, it is 9.6 cm. The Forchheimer equation is a scaled approximation to (2) given by:

$$I_H = \frac{\alpha\nu}{g{R_H}^2}u + \frac{\beta}{gR_H}u^2, \tag{4}$$

where $\alpha$ and $\beta$ are constant coefficients and $u$ is the pore velocity in the $x$ direction. The variables $u$ and $I_H$ are dependent on the physical parameters $\nu$, $g$, and $R_H$. There is no analytical derivation for the two coefficients in (4), but they are likely dependent upon the tortuosity, or interconnectedness of the pores [*Burcharth and Andersen*, 1995].

[22] Empirical estimates of $\alpha$ and $\beta$ can be found in the literature. After adjustment for different formulations of (4), the values of $\alpha$ and $\beta$ range over 11–37 and 0.08–0.34, respectively [*Englelund*, 1953; *Hall et al.*, 1995; *van Gent*, 1995; *Kells*, 1993]. Note that the commonly used forms of $\alpha$ and $\beta$ include factors of $6^2$ and 6, respectively, appropriate for spherical granules [*Burcharth and Andersen*, 1995]. In this derivation this geometrical dependence has been acknowledged explicitly through introduction of the parameter $\gamma$ in $R_H$.

[23] The large variation in $\alpha$ and $\beta$ between experiments may result from different packing arrangements [*Kells*, 1993], varying surface roughness, differences in the Reynolds number of pore flow, and differences in particle size [*Burcharth and Andersen*, 1995]. Without experimental results specific to a ridge keel, the appropriate values for these coefficients are uncertain. However, values of 20 for $\alpha$ and 0.11 for $\beta$ may be most appropriate, since they were obtained for a medium with rectangular grains, a porosity of 0.39, and a range of Reynolds number (115–1150) close to values expected in our application [*van Gent*, 1995].

### 3.2. Pore Flow Speed

[24] To determine the speed of flow through the keel, the pressure gradient across it must be known. This is related to the drag on the keel shape, to the flow speed in the upper ocean, $\bar{U}$, relative to the ice and to the density of the seawater, $\rho$, [*Cummins et al.*, 1994]:

$$C_D = \frac{\overline{P}_{upstream} - \overline{P}_{downstream}}{(1/2)\rho\left|\vec{U}\right|^2}, \tag{5}$$

where $C_D$ is the drag coefficient [*Vittal et al.*, 1977].

[25] For an obstacle in a homogeneous flow such as a river, the drag coefficient is a straightforward parameter. However, for an ice keel floating on a stratified ocean, the drag coefficient is strongly dependent on the variation of seawater density with depth. *Pite et al.* [1995] used laboratory experiments on two-layer flows to estimate the drag force on models of ice keels, using the ratio of the ice-keel depth to upper layer depth as a scaling parameter. They varied the upstream speed of the flow to obtain a range of Froude numbers representative of typical pack-ice conditions. The depths of the keel and the upper ocean layer were kept constant and in a 1:2 ratio. With increasing speed (and Froude number), the drag coefficient rose rapidly to a maximum of approximately 3.8 before decreasing to 0.2. On the basis of earlier observations of layer depths at site 2

(H. Melling, unpublished data, 1981, 1985–1996) and a representative relative current of 6.3 cm $s^{-1}$, the Froude number (0.26) calculated as by *Pite et al.* [1995] corresponds to a drag coefficient estimate of 3.5. However, natural variations in Froude number with keel draft and ice drift are likely large enough that the full range of values (0.2 to 3.8) is relevant.

[26] The drag coefficient represents the difference in pressure integrated over the upstream and downstream faces of the ice keel, but does not provide information about the distribution of pressure across the faces. The total pressure distribution must satisfy:

$$\int_h^H \Delta P(z)dz = \frac{1}{2}(H-h)C_D\rho U^2, \tag{6}$$

where $h$ is the level-ice draft, assumed here to equal the thickness of ice blocks in the ridge, and $H$ is the maximum keel draft. Pressure measurements on models of river bedforms have shown that pressure is low at the leading edge and crest of the obstacle and highest part way along the upstream face; on the downstream the pressure is relatively constant [*Vittal et al.*, 1977]. We assume a parabolic form for the pressure distribution along the upstream face of a ridge keel as the simplest shape to satisfy these constraints. The pressure drop across the keel can be written as:

$$\Delta P(z) = \frac{3C_D\rho U^2}{(H-h)^2}\left((H+h)z - z^2 - Hh\right) \tag{7}$$

[27] The horizontal gradient of pressure across the keel varies with depth because of variation in both the pressure difference and the width of the keel. The average distribution of ice with draft within a keel is an exponential function with e-folding scale $\lambda$ [*Melling and Riedel*, 1995]. Assuming the simplest smooth geometry for the envelope of a keel with this distribution of ice by draft, the keel shape is defined by its width, $\omega$, as a function of depth that has the following dependence on the full keel width, $W$:

$$\omega(z) = \frac{W\left(e^{-H/\lambda} - e^{-z/\lambda}\right)}{e^{H/\lambda} - e^{-h/\lambda}} \tag{8}$$

[28] The shape (8) is a smoothed approximation to the rough surface of a keel constructed of ice blocks. We avoid a singularity in calculation, associated with zero keel width at the crest, by using $H' = H + 0.1$ m in place of $H$ in (8). The 0.1-m value equals the grid scale of the numerical model used to calculate the ridge melting rates. The pressure gradient across the keel (Figure 3) is:

$$\frac{dP}{dx} \approx \frac{\Delta P(z)}{\omega(z)} \tag{9}$$

With a known hydraulic pressure gradient, (4) can be solved for the pore velocity, $u$ ($z$).

$$u(z) = \frac{-\alpha\nu}{2\beta R_H} + \sqrt{\frac{\nu^2\alpha^2}{4{R_H}^2\beta^2} - \frac{R_H}{\rho\beta}\frac{\partial P}{\partial x}} \tag{10}$$

[29] A substitution of (9) into (10) yields the speed of flow through the pores of the keel. As an example, the pressure gradient and percolation velocity are plotted in Figure 3 for an average shaped keel of 9-m draft ($W = 6.8H$, $\lambda = 4.2$ m) with a 0.5-m block thickness, a porosity of 0.3, relative perpendicular flow at 6.3 cm $s^{-1}$, a freezing-temperature departure of 0.18°C, the hydraulic radius given by (3), and other values as listed in Table 1. The 9-m keel draft was the largest observed during event D (Figure 1b). The pore velocity reaches its maximum value of 2.8 cm $s^{-1}$ near the keel's crest (Figure 3). The flow within the draft bin representing the maximum keel draft is not calculated, because the bottom of the keel is assumed to be a solid block of ice that is not porous.

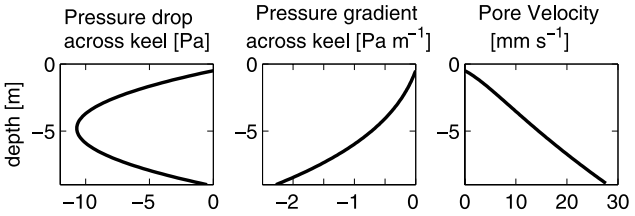


**Figure 3.** Distribution of pressure (equation 7), pressure gradient (equation 9), and pore velocity (equation 10) for a 9-m keel built from blocks 0.5 m in thickness and a current of 10 cm $s^{-1}$.

### 3.3. Heat Transfer to a Porous Media

[30] Adopting the analogue of flow through tubes, the heat transfer from the percolating fluid to the ice can be calculated with knowledge of the speed and temperature of the flow. The rate of heat transfer from the walls of a pipe to the fluid can be expressed as [*Bird et al.*, 1960]:

$$Q = \frac{Nu\kappa}{D}A\Delta T, \tag{11}$$

where $\kappa$ is the thermal conductivity, $D$ is the pipe diameter, $Nu$ is the Nusselt number, $\Delta T$ is the temperature difference between the fluid and the tube wall, and $A$ is the area of contact.

[31] Extension of this theory to porous media (e.g., a packed bed or an ice keel) is achieved by replacing the pipe area, $A$, with the surface area of the pores, $A_p$. Essentially, the porous medium can be viewed as a network of interconnecting pipes. *Bird et al.* [1960] noted the application of (11) to noncircular cross sections for turbulent flow can be accomplished by allowing $D$ to be $4R_H$. The percolating flow through the keel is most likely turbulent within the range of parameter values of this discussion.

[32] The Nusselt number in (11) is the ratio of heat transfer via forced convection in the pipe to that via conduction. For fluids where the change in viscosity with temperature is negligible, the Nusselt number for turbulent flow is [*Bird et al.*, 1960; *Knudsen and Katz*, 1958]:

$$Nu = 0.023\ \mathrm{Re}^{0.8}\ \mathrm{Pr}^{1/3}, \tag{12}$$

where the Prandtl number, Pr, is the ratio of the molecular diffusivities of momentum and heat [*Knudsen and Katz*, 1958]. The Pr value for cold seawater is 13.6 [*Holland and*

*Jenkins*, 1999]. The Reynolds number, Re, is defined here using the dimension of the interstitial voids, $4R_H$, as the length scale [*Bird et al.*, 1960]. Equation (12) is applicable where the Reynolds number exceeds 20,000. For the example of Figure 3, where the maximum speed is 2.8 cm $s^{-1}$ and $R_H$ is 5 cm, the Reynolds number is approximately 2500, too large to signify laminar flow but below the threshold for fully developed turbulence. In this transitional domain of Reynolds number, there is no simple parameterization of the Nusselt number. However, because the tortuous path of flow through a porous medium offers much opportunity for hydrodynamic instability, we use the turbulent parameterization for the Nusselt number.

[33] The surface area of ice blocks, $A_p$, within a keel volume $V_K = dx\,dy\,dz$, can be written as a function of block dimensions, $b_1h$, $b_2h$, and $h$ as outlined by *Amundrud* [2004]:

$$A_p = \frac{2(1-p)(b_1b_2 + b_1 + b_2)V_K}{b_1b_2h} = \frac{p\,dx\,dy\,dz}{R_H} \tag{13}$$

[34] Equation (11) can then be rearranged to provide $Q_m/dx$, the heat flux from the percolating flow to the ice per unit length along the $\hat{x}$ direction [*Bird et al.*, 1960]:

$$\frac{Q_m}{dx} = \frac{Nu\ \kappa\ p\ dydz}{4R_H{}^2}T_x \tag{14}$$

[35] Here $Q_m$ is the heat generating melt, and $T_x$ is the temperature above freezing of the water at $x$. Expanding (14) in terms of porosity, block thickness, and water velocity through the pores reveals a complex dependence of the form: $Q_m = fn\,(u^{0.8}, h^{-1.2}, p^{-0.2}, (1-p)^{1.2})$ suggesting that as porosity and block thickness increase, heat transfer will decrease. However, as velocity, $u$, is also a function of porosity and block thickness, the response to changes in these parameters is complex and is discussed further in section 4.

### 3.4. Ablation Within a Ridge Keel

[36] As the transfer of heat from percolating water melts the ice, meltwater is added to the flow as it travels through the keel. Considering the porous keel as a packed bed, volume flux within the ice pores can be written as:

$$(u_x - u_o)p^{2/3}dy\,dz = \int_0^x \frac{Q_m}{\rho_i L_i}dx, \tag{15}$$

where $u_o$ is the initial percolation speed, $x$ is the distance across the keel, $L_i$ is the latent heat of fusion for ice (334,000 J $kg^{-1}$), and $\rho_i$ is the ice density (920 kg $m^{-3}$). The $p^{2/3}$ factor represents the two-dimensional porosity of the keel as seen by the oncoming flow. The subscripts *o, m*, and *x* indicate input, melt or position within the keel in the $\hat{x}$ direction respectively.

[37] An analogous equation for the heat flux within the pores uses (14) and the equation $Q_o - Q_m = Q_x$ to yield:

$$T_o\rho_w u_o c_p p^{2/3}dydz - \frac{Nu\ \kappa\ p\ dydz}{4R_H{}^2}\int_0^x T_x dx = T_x\rho u_x c_p p^{2/3}dydz. \tag{16}$$

[38] This can be simplified to:

$$\int_0^x T_x dx = \frac{4R_H{}^2\rho c_p}{Nu\ \kappa\ p^{1/3}}(T_o u_o - T_x u_x) \tag{17}$$

where $c_p$ is the heat capacity of seawater (4218 J $kg^{-1}$ $K^{-1}$). Using (15) for $u_x$ and (14) for $Q_m$ in (17), the equation for the heat transfer within a packed bed is:

$$\int_0^x T_x dx + \frac{\rho c_p}{\rho_i L_i}T_x\int_0^x T_x dx = \frac{4R_H{}^2\rho c_p u_o}{Nu\ \kappa\ p^{1/3}}(T_o - T_x), \tag{18}$$

[39] Once $T_x$ is known, equation (14) provides the heat flux from the water to the keel. Figure 4 maps the flux of heat carried by the percolating flow in the $\hat{x}$ direction through the 9-m keel described earlier and the freezing-temperature anomaly of that flow.

[40] The form of equation (18) arises from the addition of the meltwater to the percolating flow. If the influx of meltwater is small enough to be neglected, $u_x$ is approximately equal to $u_o$ and (17) can be solved directly for the temperature:

$$T_x = T_o\exp[(-Nu\kappa p^{1/3}x)/(4\rho u_o c_p R_H{}^2)] \tag{19}$$

[41] A full solution of (18) for the 9-m keel and flow parameters described earlier reveals that the increase in speed caused by meltwater addition is very small; the maximum increase is 0.0007 cm $s^{-1}$ at a depth of 3.2 m, and the maximum fractional increase is less than 2% throughout the keel (Figure 5). The approximation of a constant percolation speed within a melting keel is justified in the context of the present discussion.

[42] Knowing the loss of heat from the percolating flow, the ablation within ridged ice can be calculated as the summation of ice loss over the full draft of the keel, divided by $(1-p)^{1/3}$ to represent the fraction of ice volume to total keel volume in the vertical direction. We assume that melting ice blocks are repacked by gravitational forces to maintain a constant porosity. Figure 6 displays the calculated thinning versus draft of 4-m and 9-m ice keels in comparison with the observed ablation of level ice and of the ridged ice field during the summer of 2000. Because the values calculated from observations represent a population of keels with a wide rage of draft (and potentially block thickness), the bulge in the ablation rate from observations over 3–6-m draft is not relevant at present. It may simply represent the distribution of the keel population.

[43] The calculations yield a rate of ablation much greater than that observed for level ice, but consistent with ablation measured during event D (days 192 to 207). The ablation rate increases with ridge draft, consistent with the observations of *Rigby and Hanson* [1976]. Although the calculated ablation is dependent on a choice for the (unknown) freezing-temperature departure of the upper ocean during July 2002, this choice (0.18°C) is within the range of data from other studies. Figure 6 is a persuasive indication that the ablation of ice blocks deep within ridge keels is an

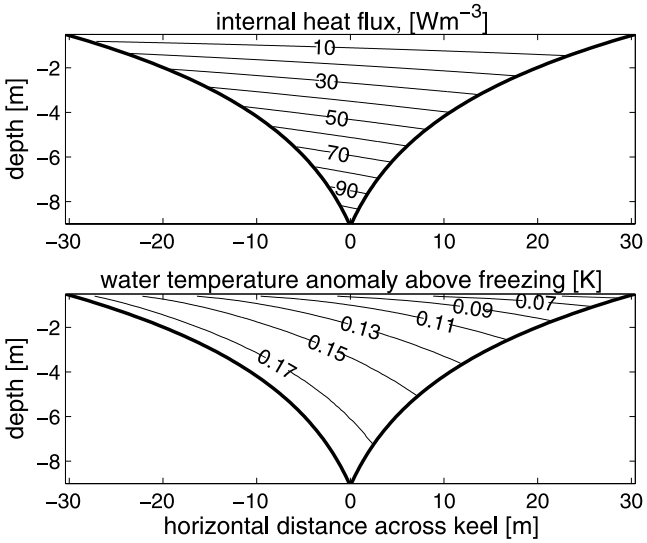


**Figure 4.** (top) Contours of the horizontal heat flux within a 9-m keel showing the decrease in heat transfer along the average direction of flow. (bottom) Contours of the freezing temperature departure, which change through the keel because of heat lost to ablation and the influx of meltwater at freezing temperature. At deeper drafts the water flows faster (from left to right on Figure 4; see Figure 3) moving further through the keel before the water reaches the freezing temperature. Keel porosity is 0.3 and block thickness is 0.5 m.

important contributor to the rapid summertime decrease in the draft of ridged ice.

[44] A more sophisticated comparison of observed and calculated ablation will be presented in section 5, where the calculations for keels of various drafts will be combined with a keel-draft distribution to yield a statistical representation of the ablation rate of ridged pack ice.

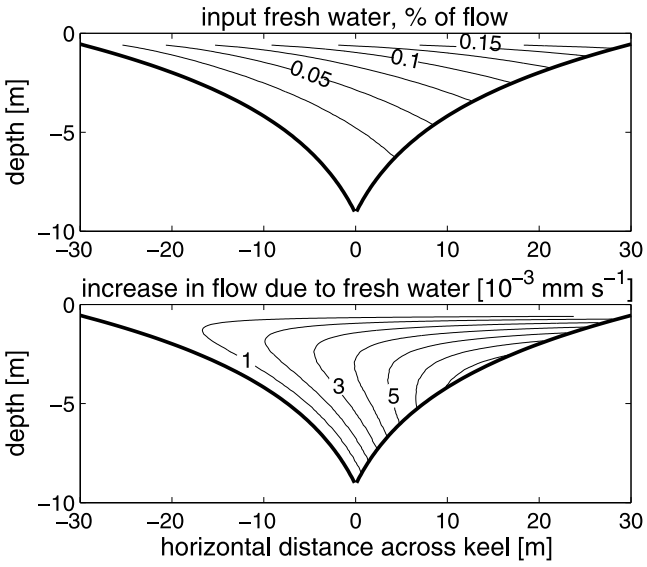


**Figure 5.** (top) Percent increase in the speed of percolating caused by meltwater addition within the keel. (bottom) Increase in flow speed. The increase in flow speed from meltwater addition is very small compared with the speed of percolation, which can exceed 25 mm s$^{-1}$ (Figure 3). Keel porosity is 0.3 and block thickness is 0.5 m.

## 4. Sensitivity of Ablation to Parameters of the Model

### 4.1. Sensitivity to Parameterizations

[45] The model of internal ridge ablation presented in section 3 is dependent upon a variety of parameters representing properties of the keel, the upper ocean, and the flow regime. Although the observed ranges in values of these parameters are established, the values appropriate to particular field observations are poorly known. In this section we investigate the impact of these uncertainties on the calculated rates of ablation and show that the basic concept of ice keel ablation via percolating flow can generate rates of ablation consistent with field data over a wide range of parameter choices.

[46] To calculate the percolating flow we have used values for the Forchheimer coefficients from a similar, but not identical, physical system. Testing of the model with values that span the entire range of published data for the Forchheimer coefficients $\alpha$ and $\beta$ (11–37 and 0.08–0.34, respectively) [*Englelund*, 1953; *Hall et al.*, 1995; *van Gent*, 1995; *Kells*, 1993] reveals that the percolating flow varies by less than 10% with $\alpha$ and by approximately 200% with $\beta$. Choices of $\alpha$ = 19 and $\beta$ = 0.09 that correspond to a packed bed of spheres, with a porosity of 0.3 similar to ice keels [*Hall et al.*, 1995], introduce only a 9% change in the percolating flow compared with *van Gent*'s [1995] values. As the values of *Hall et al.* [1995] correspond to a medium with an appropriate porosity, and the values of *van Gent*

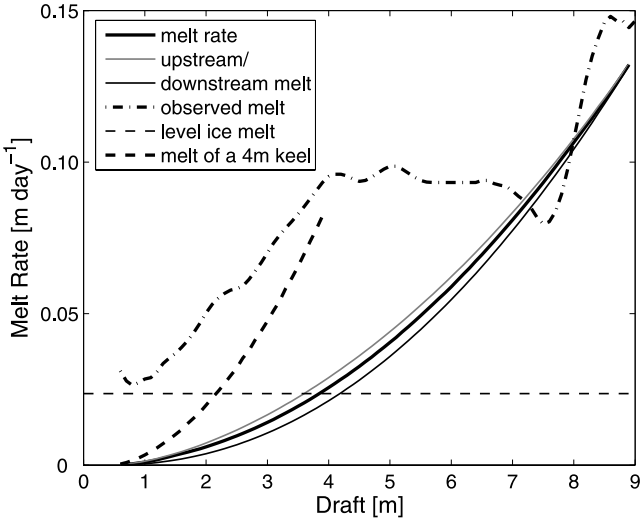


**Figure 6.** Ablation rate that results from percolation through a 9-m keel (heavy black line). Thin black lines reveal the small difference in ablation between the upstream and downstream halves of the keel. Expected ablation from level ice is shown as the thin dashed line; observed rates of ablation are shown as a thick dash-dot line. The ablation rate for a smaller 4-m keel is shown for comparison (heavy dashed line). Keel porosity is 0.3 and block thickness is 0.5 m for both keels.

[1995] correspond to irregular shaped granules that more closely resemble the blocks of ice within a keel, we conclude that our particular choices for $\alpha$ and $\beta$ do not introduce problematic uncertainty into the calculation of percolating flow.

[47] The choice of drag coefficient influences the percolating flow through its effect on the pressure head. To estimate the drag coefficient (we chose $C_D = 3.5$) we relied on laboratory tests with a model of an ice keel in stratified flow. Unfortunately, the study of *Pite et al.* [1995] investigated only the variation in drag with flow speed; much of the possible parameter space in terms of oceanic stratification and dimensional ratios remains unexplored. Moreover, the shape and internal geometry of keels and the rough, fractal form of the keel's envelope may influence drag; more research is needed. However, because the percolating flow is proportional to the square root of the drag coefficient, as in (7) and (10), the error from this uncertainty may not be dominant.

[48] The heat transfer from the water to the ice depends on the Nusselt number, Nu. We have used a parameterization valid for fully developed turbulence [*Bird et al.*, 1960] although the flow percolating through a keel may actually be in a transitional state between the laminar and turbulent regimes. A comparison of Nusselt numbers for turbulent and laminar heat transfer within tubes suggests that this uncertainty may not introduce significant error. The Nusselt number for laminar flow is given by $\mathrm{Nu} = 1.86(\mathrm{Re}\,\mathrm{Pr}\,(4R_H/l))^{1/3}$ [*Bird et. al.*, 1960], where $l$ is a length scale that we approximate as the keel width. The Nusselt number for laminar flow is within a factor of 2 of that for turbulent Nusselt flow for a 9-m keel built from 0.5-m thick blocks. Accordingly, the ability of this model to generate appreciably enhanced ablation of ice keels via percolating flow is not be greatly affected by the choice of Nusselt number.

### 4.2. Sensitivity to Ocean Parameters

[49] The purpose of this study is to demonstrate the potential for internal melt to enhance the ablation rates for thick, ridged ice. To do this, assumptions are made about the ocean current and freezing temperature departure. This section briefly explores the implications of those assumptions.

[50] In our model, the percolating flow is driven by an ocean current relative to the ice that is constant with depth. In an idealized ocean boundary layer, the speed of current will actually decrease toward the ice-water interface, thereby slowing percolation through and ablation within the upper parts of the keel. However, the concept of a steady boundary layer beneath sea ice must be used with caution. Ridge keels are steep features that frequently occupy an appreciable fraction of the boundary layer thickness. As such they significantly perturb the ocean flow. Complexity, including time dependence, arises from internal hydraulic effects associated with ocean stratification [*Pite et al.*, 1995]. The interaction of upper-ocean flow with ice topography, including percolation, is a very complicated and poorly understood topic that is beyond the scope of this research.

[51] For thick ridged ice however, the melt rate is largely determined by the relatively high melt in the lower portions of the keel (Figure 4) such that the assumption of a vertically homogeneous current does not introduce large errors in the melt rates of the thickest ice. In this context, our simple assumption of depth invariant flow is quite reasonable.

[52] For this preliminary study of ridge-keel ablation the freezing-temperature departure of the ocean water was fixed at 0.18 K, on the basis of observations at the SHEBA site. This is clearly a reasonable value, although not of course representative of all possible locations and circumstances. We emphasize that the attention of this paper is focused on the relative enhancement of ablation at deeper draft accomplished by the percolation of warm water into the keel; uncertainty in the oceanic temperature will affect the magnitude of ablation but not its dependence on draft (see (19)). We do advise caution in quantitative comparisons of data with calculations because of the uncertain value of freezing-temperature departure appropriate to the sonar observations of ablation.

[53] Moreover, the ablation of ice in saltwater involves diffusive fluxes of salt as well as of heat toward the interface. Because the diffusivity of salt in water is much lower than that of heat, meltwater lingers near the ice-water interface, lowering the salinity of seawater in contact with the ice and changing its freezing-temperature departure from the far-field value. This constraint has been discussed most recently in relation to ice in seawater by *Notz et al.* [2003]. The implication to the present discussion of neglecting salt fluxes is additional uncertainty in specifying the freezing-temperature departure, and therefore ablation rate, at the ice-water interface. The incorporation of a salt balance into our mathematical representation of ridge keel ablation by percolating flow is of high priority in future development of the concepts introduced in this paper.

### 4.3. Sensitivity to the Geometrical Factors

[54] The thickness and shape of ice blocks and the internal porosity of the ice keel are geometrical factors that influence the rate of internal ablation. The size of pores increases with the size of blocks via the hydraulic radius, $R_H$, which appears in the equations for pore velocity and heat flux. The hydraulic radius also increases with porosity. Because no information on block size or porosity can be extracted from the data acquired by ice-profiling sonar, we explore the impact of geometry on ice-keel ablation via a sensitivity analysis.

[55] Figure 7 displays the effect of varying porosity from 0.1 to 0.5 for a 9-m keel with block thickness set at 0.5 m; *Bowen and Topham* [1996] report values of ridge porosity ranging between 20 and 45%. As the porosity increases from small values, the rate of ablation initially increases as the increasing hydraulic radius permits faster percolation. However, the surface area exposed to warm water decreases as the porosity increases, as evident from (13) when rearranged to $A_P = (1-p)\gamma V_K/h$ using (3). As porosity increases above 0.4, the ablation rate stabilizes; at porosity values above 0.5, the ablation rate begins to decrease because of decreasing surface area (not shown in Figure 7). The ablation rate is thus highest where porosity is between 0.4 and 0.5, the upper bound of observed values.

[56] The sonar provides little indication of the thickness of ice blocks within keels. At the time of ridge formation, the thickness of the ice blocks piled to form the keel may be

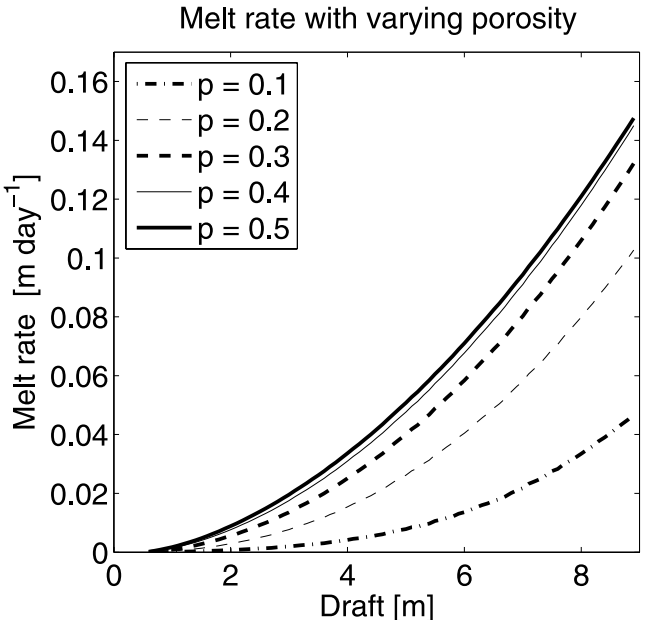


**Figure 7.** Variation in melting rates with porosity for a 9-m keel with block thickness 0.5 m.

the same as that of adjacent level ice. However, subsequent vertical growth of the level ice means that this relationship is soon invalid; in general, ice blocks in keels will be thinner than nearby level ice. While keels built from very thick sea ice do exist, they are relatively rare because of the large forces needed to build them. The bulk of pack-ice ablation will probably be associated with more common keels built from thinner blocks. However, by late winter in the Beaufort Sea there will be ridges of 20–25-m draft that have been built from ice as thick as 1–1.5 m [*Amundrud et al.*, 2004, Figure 5].

[57] The impact of block thickness on the rate of ablation is plotted in Figure 8. Block thickness is varied from 0.1 to 1.0 m to represent the range of blocks expected within keels. Melt rates increase with decreasing block sizes, as surface area increases (13) and $R_H$ decreases, until the blocks are about 25-cm thick for a keel of 9-m draft and 30% porosity. At this point, melt rates are maximized and begin to decrease, as the e-folding scale for the heat transfer (19) is dependent on $R_H^2$. As $h$ decreases past 0.25 m, $R_H^2$ becomes very small and the e-folding scale decreases such that the melt is restricted to an upstream portion of the keel. Since the ablation rate for the feature is the average melt over all ice of particular draft, its value will decrease.

[58] The external shape and the width of a keel also influence the rate of ablation. Increasing the keel width at a particular depth, either by widening the keel overall or modifying its shape, decreases the pressure gradient and the speed of percolating flow given by (10). With a wider keel and slower percolation, the e-folding scale for the heat transfer given by (19) is smaller, so that ablation occurs mainly on the upstream side of the keel.

[59] Keel width and shape parameters may not be independent of the thickness of blocks composing the keel. During keel formation, the amount of raw material available for ridging, which is equivalent to the finite extent of adjacent level ice, often prevents a keel from reaching the maximum draft permitted by ice strength [*Amundrud et al.*, 2004]. However, if a keel reaches this draft, further growth is through widening of the feature [*Hopkins*, 1998]. Therefore a wide keel may have thinner blocks than a keel of identical draft, but narrower, which was constrained by level ice extent during formation and therefore did not reach its maximum draft, $H$, of 20 $m^{1/2}$ $h^{1/2}$ [*Amundrud et al.*, 2004]. As the block thickness is such a dominant factor in determining melt rates, the errors introduced by uncertainties in keel width are secondary to concerns about block thickness.

## 5. Ablation of Ridged Pack Ice

### 5.1. Required Geometrical Statistics for Ridge Keels

[60] To apply the internal ablation model to ridged pack ice, we need to know the average keel shapes for the full range of keel drafts in the pack. We identify keels in the draft profiles of first-year ice as regions of deep draft delineated by level floes; where level floes are zones varying in draft by less than 25 cm over at least 10 m in horizontal extent [*Melling and Riedel*, 1995]. In addition, the draft at the keel edge must be at least 25 cm greater than adjacent level ice, to exclude small (less than 10 m) floes from being added to the keel flanks. This definition may classify rafted features smaller than 10 m in extent as ridged ice. However, for rafted features, which do not have the porous geometry of ridges, internal ablation processes are not applicable. To exclude such features from this analysis, we permit ablation only within keels whose maximum draft is at least three times that of surrounding level ice.

[61] Attempts to parameterize the keel width, shape, and block thickness as functions of keel depth should not be interpreted as demonstrating the dependence of these parameters on keel depth. Rather, the purpose of this section is to allow the identification of average keel geometry for use in constructing a melt model. An explanation of the

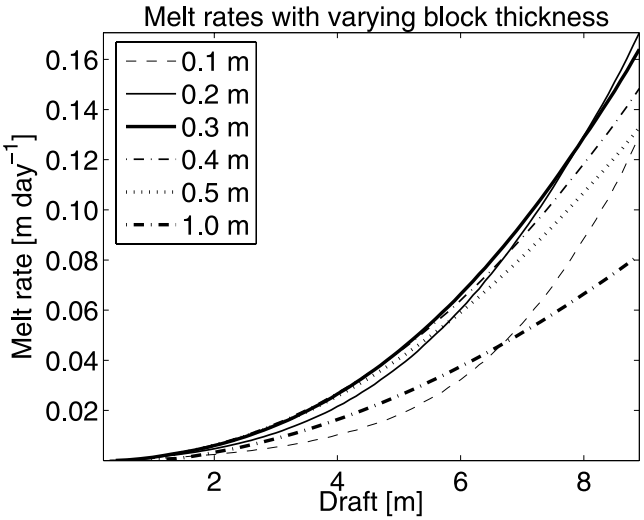


**Figure 8.** Variation in ablation rate with block thickness for a 9-m keel with a porosity of 0.3. Note that maximum ablation occurs when the block thickness is approximately 0.2 to 0.3 m.

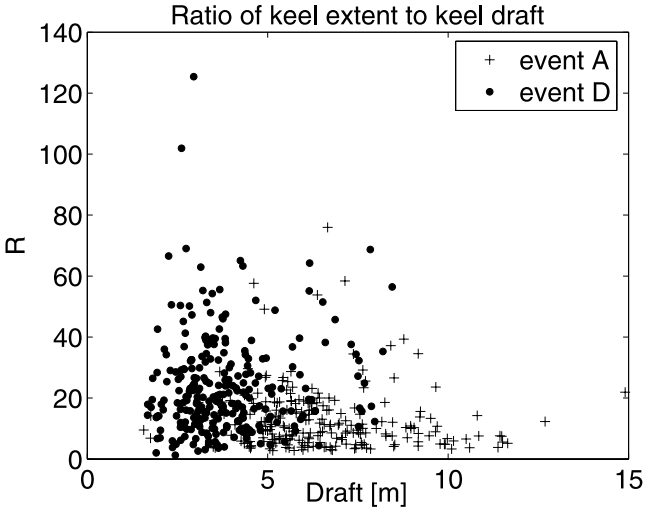


**Figure 9.** The ratio, *R*, of keel extent to keel draft for keels observed during (plus symbol) event A and (solid circle) event D.

relationship between geometrical variables and keel depth is beyond the scope of this study.

[62] The ratio, *R*, of keel extent to draft along the sonar transects averages 12.7 (standard deviation: 10.2) during event A in June 2000 (Figure 9). The average ratio is slightly higher during event D in July, perhaps because keel draft has decreased through ablation. For estimating the ablation rate, we assume that the ratio of keel extent to draft is 13, a value similar to that of *Melling and Riedel* [1995] who found keel extent to be approximately 10 times keel draft for population of 21 large keels.

[63] Assuming that keels drift past the sonar with a random orientation, the average keel width, *W*, will be less than the observed average extent by a factor that is the average over a quadrant of $(\cos\theta)^{-1}$. Here $\theta$ is the angle separating the sonar transect and the perpendicular to the keel axis. Because sec $\theta$ grows without bound at ±90 degrees, we have restricted our average to the domain of ±arctan 8. This covers more than 92% of the full domain and allows keels to be straight and uniform over at least 30 times their draft. The result is an average width of $0.52RH$ or $6.8H$, larger than the factor of 4 summarized from various field surveys by *Timco and Burden* [1997]. This discrepancy likely stems from the exclusion of irregular shaped ridges from on-ice keel survey. Corner regions may accumulate appreciably more ice rubble than linear sections [*Bowen and Topham*, 1996].

[64] The average shape of a keel can be calculated from the average distribution of draft within such features. The average histogram of draft fits a truncated exponential form, characterized by an e-folding scale $\lambda$ and a maximum draft for the population [*Melling and Riedel*, 1995; *Amundrud et al.*, 2004]. For the purpose of calculating internal ablation within a population of keels, we require the average draft histograms for keels of each maximum draft within the full range of keel drafts.

[65] An analysis of observations for average keel shape has been completed for two portions of the 1999–2000 observations, the winter and the warm season of 2000 (days 150–220). Keels were sorted by maximum draft within ±0.5-m ranges; the average histogram of draft was calculated for each keel size and the e-folding scale and its standard deviation were determined by least squares fitting to the histogram. The dependence of e-folding scale on maximum keel draft is plotted in Figure 10. The larger uncertainty at large keel draft reflects small sample size: only 107 8.5-m keels and 8 13.5-m keels were measured during 1999–2000. The linear fit is a good representation of the data, $\lambda = 0.50H - 0.32$ for $H \geq 1$ m (units are meters). *Melling and Riedel* [1995] found that the mean e-folding scale for 21 keels with drafts exceeding 20 m was 15 m. Extrapolation of the best-fit line in Figure 10 gives an e-folding scale of 12.2 m for a 25-m keel, compatible within the sampling error to the value found by *Melling and Riedel* [1995]. The values of $\lambda$ and $H$ determine keel shape using (8). We note that variation in the shape of individual keels is far greater than variation in mean shape of keels with different average draft. The rate of ablation in individual geometrically diverse keels will vary widely.

### 5.2. Ablation Over a Population of Ridges

[66] The statistical data of the previous section permit calculation of the rates of ablation for keels of average width, shape, and a range of values of maximum draft. We calculate the ablation rate of the ice pack as the sum of the ablation rates for features of each size, weighted by their relative frequency of occurrence within the pack. Because some features initially classified as ridges may actually be areas of rafting, which are not porous, we have adjusted the frequency of occurrence according to an estimate for the incidence of rafted ice, defined as features where the maximum drafts is less than three times the draft of level ice present (Figure 11); approximately 25% of deformed ice was classified as rafted.

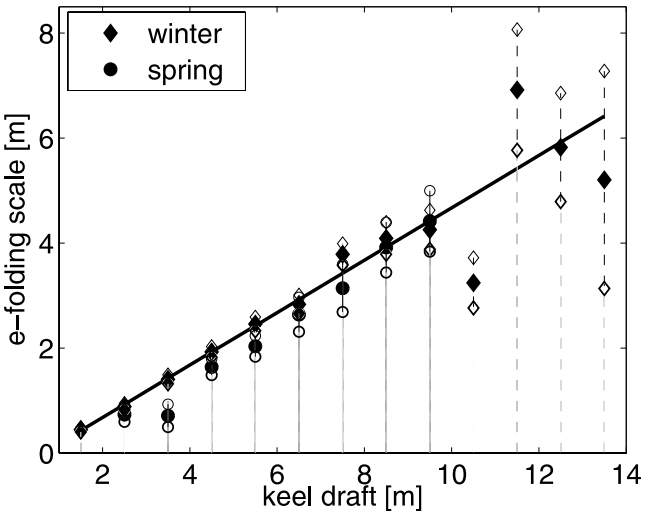


**Figure 10.** Mean e-folding scale of the histogram of ice draft for keels observed in 2000. Data are plotted from the ablation season spanning events A and D (circles) and for the entire winter 1999/2000 (diamonds). The standard deviation of the estimate has been used for the error bar. The linear best-fit line is $\lambda = 0.50H - 0.32$ (units of meters) for all periods of observation.

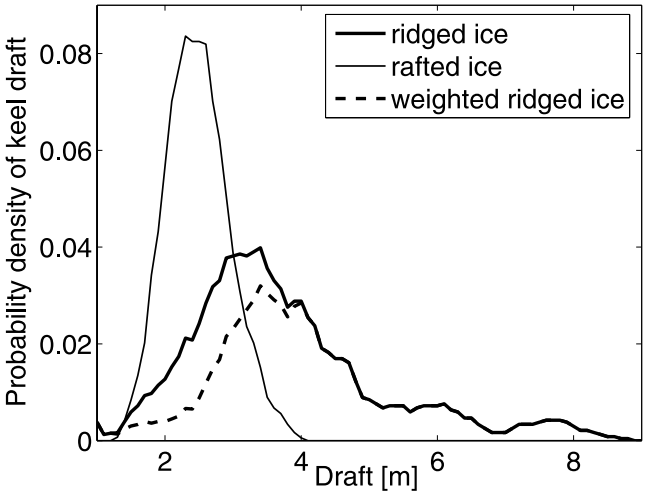


**Figure 11.** Probability density functions for the maximum draft of ridge keels (heavy line) and of rafted ice (thin line) during event D (fractions per decimeter). The function for ridge keels alone is the dashed line, representing the proportion of thick ice at that draft that is within porous ridges.

[67] Figure 12a shows the calculated rate of ablation for the pack ice observed during event D. As anticipated, the loss of ice via ablation within keels is much greater than the observed ablation of level ice. The sum of the calculated loss of ice within keels and the measured loss from level ice is quite similar to the observed ablation and its variation with draft. Note that exact agreement is not expected as the observed ablation rate is the net result of ablation and ridging processes. The internal melt is just one contributor to the overall evolution of ridged ice. The calculated ablation during event A (days 154 to 173) is also similar to field measurements in magnitude and draft dependence (Figure 12b); for calculations during this earlier event, the value 0.09°C was selected as the freezing temperature departure of the upper ocean. This is in the middle range of values (0.07–0.11°C) observed beneath ice at the SHEBA site during much the same time period (days 155 to 175). The comparisons in Figure 12 argue strongly for the importance of percolating warm seawater in accelerating the ablation of ridged first-year pack ice.

[68] The poor knowledge of the freezing temperature departure within the under-ice layer hinders a rigorous quantitative comparison of observations and theory. Our assumed values (0.18°C and 0.09°C for events D and A, respectively) are consistent with observations elsewhere at other times. However, much larger values are possible: the freezing temperature departure at the land-fast ice edge of the Beaufort Sea on 3 June 1987 ranged over 0.35–0.7°C, more than twice the values assumed here. Such high values would promote ablation at proportionately higher rates.

## 6. Implications and Conclusions

[69] A new mechanism for the rapid ablation of first-year ice ridges has been explored. The mechanism accelerates the loss of pack-ice mass in summer as a consequence of ablation deep within the porous keels of ridges. A numerical formulation of this mechanism yields a rate of thinning that increases with ice draft consistent with observations in the Beaufort Sea in summer. The ablation of keels by this process may well continue at a reduced rate during the cold months, when sensible heat is available to deep keels via the depression of freezing temperature through pressure and via penetration into the halocline.

[70] The accelerated ablation of ridged ice through deterioration of porous keels is not currently represented in large-scale models of polar oceans. In view of the large magnitude of the enhancement (up to ten times), and the

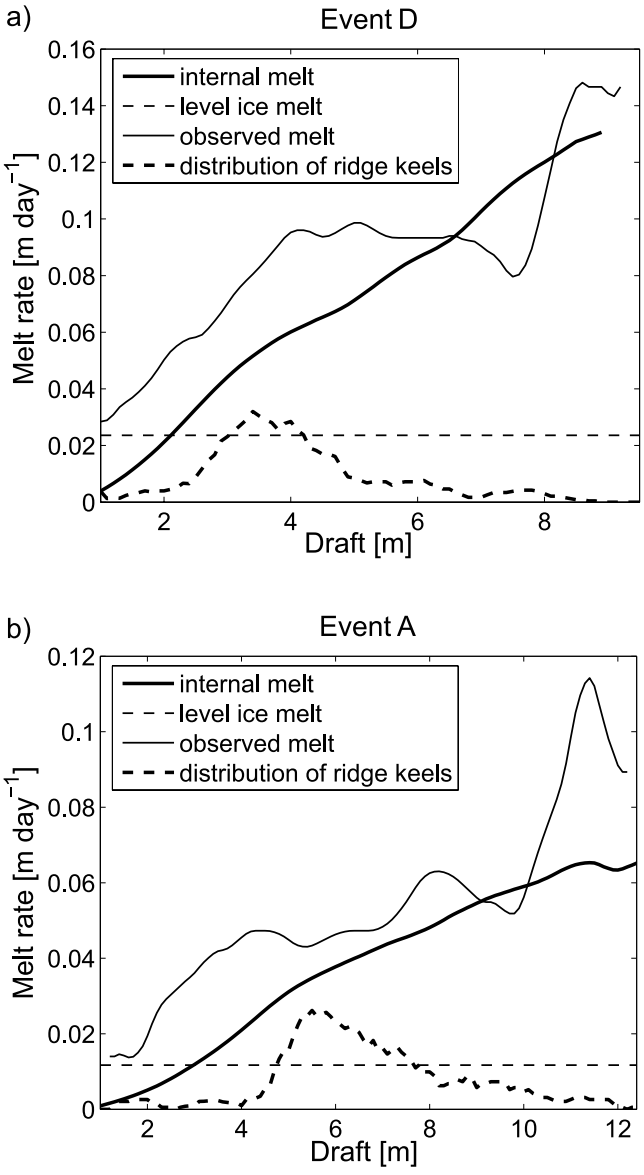


**Figure 12.** Ablation rate within ridged ice during (a) event D and (b) event A. The enhanced ice loss rate caused by internal ablation (heavy black line) increases the ablation rate above that for level ice (thin dashed line) to match the observed rate (thin line). The probability density function for ridged ice (fraction per decimeter) is indicated by the heavy dashed line.

large areal fraction of ridged ice (typically more than one half), this oversight needs examination.

[71] The model stems from recognition of the complex, small-scale geometry of ice ridges. These features are loosely stacked heaps of ice blocks that have broken from surrounding level floes during ridge-building events. As such, they do not seriously impede the penetration of warm seawater from the upper ocean deep into the ridge keel; under many circumstances ablation may occur through the full width of the keel. Use of the model is hindered by poor information on the values for important physical parameters, such as block size and the temperature of the oceanic boundary layer under ice. Its use in this study has been semiquantitative.

[72] The model has been evaluated against the observed rate of ablation of first-year pack ice in the Beaufort Sea during summer; data were acquired by ice-profiling sonar mounted on subsea moorings. With reasonable choices for oceanic freezing-temperature departure, flow relative to the ice and the block size within ridges, the model easily reproduces both the magnitude and draft dependence of observed ablation.

[73] Conventional theory for flow through packed beds indicates that as much as 20% of the incident boundary flow may percolate through the keel, with the remaining fraction diverted below or around it. The percolating fraction and its impact on ablation are sensitive to the size and packing of the ice blocks within the keel. The ablation rate is most rapid when the porosity of the keel is 40–50% and block thicknesses about 25 cm. The greatly enhanced rate of ablation of ridges is primarily a consequence of the dramatic increase in the ratio of surface area to volume of unconsolidated versus solid ice features.

[74] The lack of information on the block thickness distribution in ice ridges is a significant shortcoming of present knowledge of deformed pack ice. In our calculations, we assumed that blocks were 50-cm thick, more than twice the value promoting most rapid ablation. Moreover, we have worked with keel shapes and widths that are averages over large populations. Individual features differ greatly in these respects. A more comprehensive theory of pack-ice ablation would incorporate variability in block sizes and keel shapes into the calculations of percolating flow and heat transfer.

[75] The under-ice flow has been greatly simplified in this work. Current applications of hydraulics theory to under-ice flows have not recognized the existence of percolating flow, and have adopted greatly oversimplified and smoothly varying shapes for the ridge keels. Further lab and numerical modeling studies of two-layer hydraulic flow under ridged ice are needed to obtain better estimates of drag coefficients for a wide range of porous and variable shaped keels.

[76] The eventual consolidation of porous first-year ice ridges into solid multiyear features of smoother relief is poorly understood. The consolidation of ridge keel by freezing in winter occurs at a rate only about twice that of level ice [*Lepparanta and Hakala*, 1992; *Høyland*, 2002; *Veitch et al.*, 1991]. At such slow rates, freezing cannot solidify an entire keel in one winter. *Rigby and Hanson* [1976] observed that voids in ridge keels became slush filled in summer, implying that thawing might be a key aspect of the process of consolidation. We speculate that internal ablation due to percolating flow may be important to the consolidation of ridge keels. Blocks in the keel will be softened, thinned and reshaped by internal ablation, permitting closer repacking under the influence of buoyancy forces. In this work, we have assumed this repacking does not occur in the early summer, guided by the observations of *Lepparanta et al.* [1995], who noted little change in porosity in the early stages of ablation in the Baltic Sea. The internal melt model may not be applicable in the later summer if melt has changed the structure of the ridge significantly. Further research into the potential for melt to lead to collapse of a porous ridge and subsequent consolidation during the following winter would be of great value.

[77] **Acknowledgments.** The observational base for this project has accumulated over more than a decade, funded by the Federal Panel on Energy Research and Development, with support from the Department of Fisheries and Oceans Canada, the Canadian Coast Guard, and the Polar Continental Shelf Project. The outstanding talents of Syd Moorhouse, Ron Cooke, Paul Johnston, Peter Gamble, and Ron Lindsay in engineering development and in fieldwork are gratefully acknowledged. We thank Edmand Fok for software development and Dave Riedel for his diligence in the careful processing of sonar data and for his advice and support throughout this research. Funding for this study was provided by NSERC and the Department of Fisheries and Oceans Canada (T.A., R.G.I.) and by the Federal Panel on Energy Research and Development in relation to northern hydrocarbon development and climate change impact on the energy sector (H.M.).

## References

Amundrud, T. L. (2004), Geometrical constraints on the formation and melt of ridged sea ice, Ph.D. thesis, Univ. of B. C., Vancouver, Can.

Amundrud, T. L., H. Melling, and R. G. Ingram (2004), Geometrical constraints on the evolution of ridged sea ice, *J. Geophys. Res.*, *109*, C06005, doi:10.1029/2003JC002251.

Batchelor, G. K. (1967), *An Introduction to Fluid Dynamics*, Cambridge Univ. Press, 615 pp., New York.

Bird, R. B., W. E. Stewart, and E. N. Lightfoot (1960), *Transport Phenomena*, 779 pp., John Wiley, Hoboken, N. J.

Bowen, R. G., and D. R. Topham (1996), A study of the morphology of a discontinuous section of a first year Arctic pressure ridge, *Cold Reg. Sci. Technol.*, *24*, 83–100.

Burcharth, H. F., and O. H. Andersen (1995), On the one-dimensional steady and unsteady percolating flow equations, *Coastal Eng.*, *24*, 233–257.

Cummins, P. F., D. R. Topham, and H. D. Pite (1994), Simulated and experimental two-layer flows past isolated two dimensional obstacles, *Fluid Dyn. Res.*, *14*, 105–119.

Englelund, F. A. (1953), *On the Laminar and Turbulent Flows of Ground Water Through Homogeneous Sand*, Dan. Acad. of Tech. Sci., Lyngby, Denmark.

Gill, A. E. (1982), *Atmosphere-Ocean Dynamics*, 662 pp., Elsevier, New York.

Hall, K. R., G. M. Smith, and D. J. Turcke (1995), Comparison of oscillatory and stationary flow through porous media, *Coastal Eng.*, *24*, 217–232.

Holland, D. M., and A. Jenkins (1999), Modelling thermodynamic ice-ocean interactions at the base of an ice shelf, *J. Phys. Oceanogr.*, *29*, 1787–1800.

Hopkins, M. (1998), Four stages of pressure ridging, *J. Geophys. Res.*, *103*(C10), 21,883–21,891.

Høyland, K. V. (2002), Simulations of the consolidation process in first year sea ice ridges, *Cold Reg. Sci. Technol.*, *34*, 143–158.

Johnston, M., and R. Frederking (2001), *Decay of First-Year Sea Ice: A Second Season of Field Measurements*, *Tech. Rep. HYD-TR-066*, 18 pp., Natl. Res. Counc., Ottawa, Canada.

Kells, J. A. (1993), Spatially varied flow over rockfill embankments, *Can. J. Civ. Eng.*, *20*(5), 820–827.

Knudsen, J. G. and D. L. Katz (1958), *Fluid Dynamics and Heat Transfer*, 576 pp., McGraw-Hill, New York.

Lepparanta, M., and R. Hakala (1992), The structure and strength of first year ice ridges in the Baltic Sea, *Cold Reg. Sci. Technol.*, *20*, 295–311.

Lepparanta, M., M. Lensu, P. Kosloff, and B. Veitch (1995), The life story of a first-year sea ice ridge, *Cold Reg. Sci. Technol.*, *23*, 279–290.

McPhee, M. G. (2002), Turbulent stress at the ice/ocean interface and bottom surface hydraulic roughness during the SHEBA drift, *J. Geophys. Res.*, *107*(C10), 8037, doi:10.1029/2000JC000633.

Melling, H. (1998), Detection of features in first-year pack ice by synthetic aperture radar (SAR), *Int. J. Remote Sens.*, *19*(6), 1223–1249.

Melling, H. (2002), Sea ice of the northern Canadian Arctic archipelago, *J. Geophys. Res.*, *107*(C11), 3181, doi:10.1029/2001JC001102.

Melling, H., and D. A. Riedel (1995), The underside topography of sea ice over the continental shelf of the Beaufort Sea in the winter of 1990, *J. Geophys. Res.*, *100*(C7), 13,641–13,653.

Melling, H., and D. A. Riedel (1996), Development of seasonal pack ice in the Beaufort Sea during the winter of 1991–1992: A view from below, *J. Geophys. Res.*, *101*(C5), 11,975–11,991.

Melling, H., D. R. Topham, and D. A. Riedel (1993), Topography of the upper and lower surfaces of 10 hectares of deformed sea ice, *Cold Reg. Sci. Technol.*, *21*, 349–369.

Notz, D., M. G. McPhee, M. G. Worster, G. A. Maykut, K. H. Schlünzen, and H. Eicken (2003), Impact of underwater-ice evolution on Arctic summer sea ice, *J. Geophys. Res.*, *108*(C7), 3223, doi:10.1029/2001JC001173.

Pite, H. D., D. R. Topham, and B. J. van Hardenberg (1995), Lab measurements of the drag force on a family of two-dimensional ice keel models in a 2-layer flow, *J. Phys. Oceanogr.*, *25*(12), 3008–3031.

Rigby, F. A., and A. Hanson (1976), Evolution of a large Arctic pressure ridge, *Arctic Ice Dyn. Joint Exp. Bull.*, *34*, 43–71.

Rothrock, D. A. (1986), Ice thickness distribution—Measurement and theory, in *The Geophysics of Sea Ice*, *NATO Adv. Study Inst. Ser., Ser B*, vol. 146, edited by N. Untersteiner. chap. 8, pp. 551–575, Springer, New York.

Sayed, M., and R. M. Frederking (1989), Measurements of ridge sails in the Beaufort Sea, *Can. J. Civ. Eng.*, *16*, 16–21.

Schramm, J. L., G. M. Flato, and J. A. Curry (2000), Toward the modelling of enhanced basal melting in ridge keels, *J. Geophys. Res.*, *105*(C6), 14,081–14,092.

Skyllingstad, E. D., C. A. Paulson, W. S. Pegau, M. G. McPhee, and T. Stanton (2003), Effects of keels on ice bottom turbulence exchange, *J. Geophys. Res.*, *108*(C12), 3372, doi:10.1029/2002JC001488.

Timco, G. W., and R. P. Burden (1997), An analysis of the shapes of sea ice ridges, *Cold Reg. Sci. Technol.*, *25*, 65–77.

van Gent, M. R. A. (1995), Percolating flow through rubble-mounded material, *J. Waterw. Port Coastal Ocean Eng.*, *3*, 176–181.

Veitch, B., P. Kujala, P. Kosloff, and M. Lepparanta (1991), Field measurements of the thermodynamics of an ice ridge, *Rep. M-114*, i–vi, 1–33, Lab. of Nav. Archit. and Mar. Eng., Helsinki Univ. of Technol., Espoo, Finland.

Vittal, N., K. G. Ranga Raju, and R. J. Garde (1977), Resistance of two-dimensional triangular roughness, *J. Hydraul. Res.*, *15*, 19–35.

Wadhams, P. (1992), Sea ice thickness distribution in the Greenland Sea and Eurasian Basin, May 1987, *J. Geophys. Res.*, *97*(C4), 5331–5348.

S. E. Allen and R. G. Ingram, Department of Earth and Ocean Sciences, University of British Columbia, 6339 Stores Boulevard, Vancouver, BC, Canada, V6T 1Z4.

T. L. Amundrud, Fisheries Research Services Marine Laboratory, P.O. Box 101, Victoria Road, Aberdeen AB11 9DB, UK. (t.amundrud@marlab.ac.uk)

H. Melling, Institute of Ocean Sciences, Department of Fisheries and Oceans, P.O. Box 6000, Sidney, BC, Canada, V8L 4B2.